

Geometric Phase and Intensity-Controlled Extrinsic Orbital Angular Momentum of Off-Axis Vortex Beams

Satyajit Maji[✉], Philip Jacob[✉], and Maruthi M. Brundavanam^{✉*}

Department of Physics, Indian Institute of Technology Kharagpur, 721302, West Bengal, India



(Received 6 August 2019; revised manuscript received 19 September 2019; published 22 November 2019)

Off-axis vortex beams are generated by superposing a Gaussian beam onto a symmetric optical vortex beam of unit topological charge in a single-path interferometer with a control of their relative intensities and phases. The radial displacement of the point vortex from the center of the beam is controlled by varying the relative intensity of the superposed beams, while the azimuthal displacement of the vortex is controlled by the phase difference between the superposed beams. This phase difference is employed through the Pancharatnam-Berry geometric phase by different cyclic evolutions of the polarization states of the superposed beams on the Poincaré sphere. Interferometric field reconstruction of the resultant beams from experiment, simulation, and numerical calculations are used to obtain the transverse linear momentum density. The net transverse linear momentum vector and the resulting extrinsic orbital angular momentum in an off-axis vortex beam is demonstrated to be related to the radial and azimuthal position of the vortex across the beam. Controlling the Pancharatnam-Berry geometric phase and intensity ratio of the component beams is thus proposed as an effective and robust technique to tune the extrinsic orbital angular momentum of off-axis vortex beams. The presented results can be useful in applications ranging from optical manipulation of trapped microparticles, controlling micromachines using light with orbital angular momentum to enabling more flexibility in superresolution microscopy and controlled asymmetric interaction of light with atom, molecule, and Bose-Einstein condensate.

DOI: [10.1103/PhysRevApplied.12.054053](https://doi.org/10.1103/PhysRevApplied.12.054053)

I. INTRODUCTION

Optical vortex (OV) beams carrying orbital angular momentum (OAM), characterized by azimuthal phase dependence and phase singularities have developed significantly during the last three decades after their first study by Les Allen *et al.* in 1992 [1]. The vast applications of OV beams include their use in optical trapping and micromanipulation [2], optical communication [3], super resolution [4], and phase-contrast imaging [5], to name a few. OV beams generated from fractional helicoid phase step are of special interest in recent times due to continuous tunability of the average OAM and controllable OAM spectrum. The control of radial and azimuthal position of the vortex point across the beam is demonstrated using fractional OV beams with tuning of the fractional order of the dislocation and Gouy phase [6] and also using an off-axis spiral-phase element [7]. However, the use of different computer-generated holograms and the moving optical system or holographic element limits its usage as a robust system to control the vortex position and the resulting OAM.

The nature of the OAM carried by optical beams is now being termed as quasi-intrinsic [8], as they are not independent of the axis about which OAM is calculated unlike their spin counterpart, which is confirmed to be purely intrinsic. The underlying reason behind the emergence of extrinsic OAM is the presence of a net linear momentum in the transverse plane, which clearly results in the axis-dependent value of OAM. So, the natural choice of beam axis as the axis for calculation of OAM does not suffice in these cases [8–10]. However, the intrinsic part of the OAM can still be extracted if an axis could be found with respect to which the beam has zero net transverse linear momentum (TLM). Any choice of calculated axis parallel to this new axis, will result in the intrinsic OAM component [10,11]. The extrinsic nature of the OAM has been the object of investigation in some recent reports, especially in the context of off-axis asymmetric vortex beams [6,7,12]. Irrespective of their generation method, be it superposition of OAM beams, off-axis illumination, or use of a fractional-order spiral-phase element, the extrinsic OAM is an integral part of off-axis vortex beams.

The superposition of different OAM beams, both using a two-path interferometer and off-axis illumination of a grating hologram has been carried out previously and their usefulness has been proposed in quantum cryptography

*bmmanoj@phy.iitkgp.ac.in

[13]. Another recent study showing the generation of off-axis vortices using off-axial placement of the spiral-phase plate provides a relation for the normalized OAM of the beam as a function of the displacement of the vortex from the beam axis [7]. However, as already noted, any two-path interferometer setup or a moving component setup is prone to undesired instability because of inherent limitations such as misalignment and air currents.

In this study, we report the convenient and robust generation of an optical beam with a tunable off-axis vortex both in radial and azimuthal degrees of freedom. This is achieved in a single-path superposition of a symmetric OV beam with a beam in the fundamental Gaussian mode exploiting the polarization-sensitive response of a nematic liquid-crystal spatial light modulator (SLM). The resultant beam has a point vortex whose radial displacement from the beam axis depends on the relative intensities of the interfering vortex and Gaussian beams.

The azimuthal phase dependence of OV beams indicates the possibility of tuning the azimuthal position of the vortex by tuning the phase difference of the superposed beams. To the best of our knowledge, only a few studies have been reported where the required phase difference between OAM beams is brought about by utilizing the geometric phase (GP) due to the cyclic evolution of the beams on the parametric space of the beam parameter (beam width) [6] and spatial modes' parametric space [14]. However, surprisingly, no such studies have reported the use of the GP due to their evolution on the parametric space of polarization, namely, the Poincaré sphere, which is popularly known as the Pancharatnam-Berry geometric phase (PB GP) [15,16]. In this study, we control the PB GP of the two component beams in a common path by using a sequential quarter-wave plate (QWP)-polarizer-half-wave plate (HWP) (QPH) combination. The setup can, in fact, also be employed to utilize as well as measure the PB GP [17]. Use of GP has the advantages of being more compact, wavelength independent, and less sensitive to misalignment errors than any other previously reported methods. Thus, robustness of GP potentially enables the use of such a technique in quantum photonic components, which will be less prone to errors [18].

GP plays an important role in the spin-orbit-coupling effects in light such as the spin Hall effect, spin-controlled shaping of light at anisotropic structures, metasurfaces, and the spatial and angular (Goos-Hänchen and Imbert-Fedorov) shifts during reflection at the dielectric interfaces. All these are a manifestation of the coupling or conversion of spin angular momentum (SAM) to intrinsic or extrinsic OAM [19]. These effects are non-negligible especially in the nonparaxial regime because of strong spin-orbit coupling. Most of these phenomena are explained by different symmetry-breaking events happening at the optical interfaces or inside inhomogeneous media. In this paper, we demonstrate how an apparently

simple superposition of two completely symmetric fields give rise to an asymmetry and thus results in an extrinsic OAM in free-space propagation without any interface or inhomogeneous media. The magnitude and direction of the asymmetry is controlled by relative amplitudes of superposition and GP. We also explain this symmetry breaking from the interference of the component plane waves with different propagation vectors of the two beams.

Experimental reconstruction of the field using the interferometric method is adopted to estimate the transverse Poynting vector distribution and OAM content of the generated beams. Computer simulations and numerical calculations are also performed to support the experimental results. When integrated across the beam, the resulting net TLM (NTLM) dictates the extrinsic OAM carried by the beam. The variation of the NTLM possessed by an off-axis OV beam as a function of the radial displacement of the vortex from the beam axis is studied. It is also demonstrated that the orientation of the NTLM vector of the beam superposition can be tuned by the introduction of suitable PB geometric phase in each of the two orthogonal polarization components. Thus, robust tuning of the total OAM and extrinsic OAM is achieved.

In superresolution [stimulated emission depletion (STED)] microscopy [4], where the region of interest is changing, for example, in live-cell superresolved microscopy [20], it is desirable to move the dark core of the STED beam along small distances. The precise tuning of the vortex position in both radial and azimuthal degrees of freedom, as achieved here, enables following the region of interest with great flexibility without moving any optical component. Also, measurement of the acquired GP difference by two different polarization components in a physical system can be achieved simply by measuring the rotation of the vortex position in the proposed configuration. The demonstrated way to easily control the amount of the extrinsic OAM and relative proportion of intrinsic and extrinsic OAM can find direct application in driving micromachines by light and in optical manipulation of trapped microparticles. This method can also enable controlled asymmetry of the OAM beam in the interaction of light with atoms or molecules and in Bose-Einstein condensates (BECs) [21,22].

II. THEORETICAL DETAILS

A. PB geometric phase

In 1984, Berry described, in his landmark paper, that the slow (adiabatic) cyclic variation of a quantum system in an eigenstate makes it acquire a geometric phase depending on the path of intermediate states [23], along with the familiar dynamical phase. Berry's phase was soon generalized for nonadiabatic, noncyclic, and nonunitary transformations [24,25]. For the case of change in the polarization states of light, which is represented by

a curve on the surface of the Poincaré sphere, the geometric phase acquired is equivalent to half the value of the solid angle subtended by the closed path of states traversed, at the center of the sphere, and is referred to as the Pancharatnam-Berry geometric phase [15,16,26].

This is usually demonstrated with the help of Jones calculus, where two-component column vectors, called Jones vectors represent the polarization state of light and the matrices represent optical components that alter the phase or polarization state of light incident on them. The amount of PB GP due to the effect of a sequential QPH combination on two different polarized lights is obtained below, where the QWP is at $\pi/4$, the polarizer at θ , and the HWP at $\theta/2$ with respect to the horizontal linear polarization state.

Taking horizontal (H) and vertical (V) linear polarization states as the basis states, we have for an input H -polarized beam $|E\rangle_{\text{in},1} = E_H \begin{bmatrix} 1 \\ 0 \end{bmatrix}$, the output after a sequential QPH combination as

$$\begin{aligned} |E\rangle_{\text{out},1} &= J_{\text{HWP}}(\theta/2) J_P(\theta) J_{\text{QWP}}(\pi/4) |E\rangle_{\text{in},1} \\ &= \frac{1}{\sqrt{2}} E_H \exp \left\{ -i \left(\theta - \frac{\pi}{4} \right) \right\} \begin{bmatrix} 1 \\ 0 \end{bmatrix}. \end{aligned} \quad (1)$$

Similarly, for a input V -polarized beam $|E\rangle_{\text{in},2} = E_V \begin{bmatrix} 0 \\ 1 \end{bmatrix}$, the QPH action gives a H -polarized output beam represented as

$$|E\rangle_{\text{out},2} = \frac{1}{\sqrt{2}} E_V \exp \left\{ +i \left(\theta - \frac{\pi}{4} \right) \right\} \begin{bmatrix} 1 \\ 0 \end{bmatrix}. \quad (2)$$

The difference of PB GP between the H -polarized $|E\rangle_{\text{out},1}$ and $|E\rangle_{\text{out},2}$ is thus $\text{GP}_2 - \text{GP}_1 = |2\theta - \pi/2|$.

B. Transverse linear momentum

To derive the expression of TLM density and the magnitude of NTLM of the resultant beam, the field expressions of the OAM beams can be taken to be simply [27]

$$\psi_{l_i} = \exp \left(-\frac{r^2}{\omega_{l_i}^2} \right) (x + iy)^{l_i}, \quad (3)$$

where $i = 0, 1$ gives $l_0 = 0$ implying Gaussian beam and $l_1 = 1$ implying OV beam of topological charge 1. ω_0 and ω_1 are the half width of the Gaussian and OV beam, respectively, and $r^2 = x^2 + y^2$ is the radial variable. The superposition of the two beams with relative amplitudes $\sin(\alpha)$ and $\cos(\alpha)$ with a relative phase of δ between them is given as

$$\psi = a \sin(\alpha) \psi_0 + b \cos(\alpha) \psi_1 \exp(i\delta),$$

$$\begin{aligned} &= a \sin(\alpha) \exp \left(-\frac{r^2}{\omega_0^2} \right) \\ &\quad + b \cos(\alpha) \exp \left(-\frac{r^2}{\omega_1^2} \right) (x + iy) \exp(i\delta). \end{aligned} \quad (4)$$

Here a and b represent the maximum amplitudes in the beam cross section of a Gaussian and OV beam, respectively. As the half width of the OV beam of topological charge l scales as $\sqrt{l+1}$ with respect to the half width of the Gaussian beam [28], then $\omega_1 = \sqrt{2}\omega_0$.

The expression of TLM density is given by [29]

$$\begin{aligned} p_{\perp} &= \frac{i\epsilon_0}{2\omega} \text{Im} (\psi^* \partial \psi) = \frac{i\epsilon_0}{2\omega} \text{Im} \left\{ a \sin^2(\alpha) \psi_0^* \partial \psi_0 \right. \\ &\quad \left. + b \cos^2(\alpha) \psi_1^* \partial \psi_1 + ab \sin(\alpha) \cos(\alpha) \right. \\ &\quad \times \left. [e^{i\delta} \psi_0^* \partial \psi_1 + e^{-i\delta} \psi_1^* \partial \psi_0] \right\}, \end{aligned} \quad (5)$$

$$\begin{aligned} p_x &\propto \text{Im} (\psi^* \partial_x \psi) = \exp \left(-\frac{r^2}{\omega_0^2} \right) [-b^2 \cos^2(\alpha) y] \\ &\quad + \exp \left(-\frac{3r^2}{\omega_0^2} \right) ab \sin(\alpha) \cos(\alpha) \\ &\quad \times \left\{ \sin(\delta) + \frac{x^2}{\omega_0^2} [x \sin(\delta) + y \cos(\delta)] \right\}, \end{aligned} \quad (6a)$$

$$\begin{aligned} p_y &\propto \text{Im} (\psi^* \partial_y \psi) = \exp \left(-\frac{r^2}{\omega_0^2} \right) [b^2 \cos^2(\alpha) x] \\ &\quad + \exp \left(-\frac{3r^2}{\omega_0^2} \right) ab \sin(\alpha) \cos(\alpha) \\ &\quad \times \left\{ \cos(\delta) + \frac{y^2}{\omega_0^2} [x \sin(\delta) + y \cos(\delta)] \right\}, \end{aligned} \quad (6b)$$

where “Im” implies the imaginary part of the term in parenthesis. p_x and p_y represent the x and y component of p_{\perp} . From the distribution of p_x and p_y , the transverse distribution of Poynting vector and the NTLM can be calculated. When integrated over the beam cross section, the first term and the terms containing odd powers of x or y inside the parenthesis in both p_x and p_y becomes zero (by virtue of being a odd function, as the integration runs from $-\infty$ to ∞ in both x and y) and thus make no contribution to the NTLM. However, the term containing no x or y , i.e., $ab \sin(\alpha) \cos(\alpha) \sin(\delta)$ in Eq. (6a) and $ab \sin(\alpha) \cos(\alpha) \cos(\delta)$ in Eq. (6b) gives a finite NTLM, unless $\alpha = 0$ (therefore $\psi = \psi_1$) or $\alpha = \pi/2$ (therefore $\psi = \psi_0$), which imply only OV beam or only Gaussian beam, respectively. Both of these, of course, have a zero

NTLM because of the perfect cylindrical symmetry. In general, the magnitude of the NTLM for the superposed beams is thus $ab \sin(\alpha) \cos(\alpha)$ and its direction is set by the value of δ . For $\delta = 0$ or π it is directed along the y direction and for $\delta = \pi/2$ or $3\pi/2$, the NTLM vector is directed along the x direction. In this study, the value of δ is set by PB GP using the sequential QPH combination as is experimentally demonstrated below.

A more realistic model for the field generated by diffraction of a Gaussian beam from a spiral-phase plate is available in the literature that uses the modified Bessel function and is given as [29,30]

$$\Psi'_n(r, \phi) = (-i)^{n+1} \exp(in\phi) \left(\frac{k\omega^2}{4f} \right) \sqrt{2\pi x} \times \exp(-x) \left[I_{\frac{(n-1)}{2}}(x) - I_{\frac{(n+1)}{2}}(x) \right]. \quad (7)$$

Here I_v is the modified Bessel function of order v and $x = \frac{1}{2}(k\omega r/2f)^2$, where f is the focal length of the Fourier lens used to get the far-field profile.

Although Eq. (7) is a more realistic model of the experimental field profile, it is found to be much harder to obtain an analytic formula for the TLM density using this model than using Eq. (4). As a result, the analytic formula of NTLM using this model also becomes more complex. We stick to the simple model of Eq. (4) in favor of the resulting simple expression of TLM density and NTLM for the purpose of this Paper. And it is shown later in Sec. IV that the used simple model of Eq. (4) gives a similar match with the experimental plots when compared to the more realistic model of Eq. (7).

III. EXPERIMENTAL DETAILS

The schematic setup for the single-path generation of optical beams with a nested off-axis vortex, as shown in Fig. 1, comprises of a He-Ne continuous-wave laser source, a HWP to tune the plane of polarization, a phase-only modulation liquid-crystal SLM, and a QPH set to tune the PB GP. The resultant off-axis OV beam is again interfered with a separate expanded Gaussian reference beam derived from the same source in a Mach-Zehnder interferometer and a CCD camera captures images of the interference fringe pattern. From the interferogram analysis, the field information of the envisaged beam is obtained.

The SLM employed is a computer-controlled silicon-based nematic liquid-crystal microdisplay (Pluto from Holoeye), which acts as a phase-only SLM. When the SLM displays a typical phase function through the calibrated gray-level colormap, only the polarization component of the incoming light along a particular direction (in this case, along the longer dimension of the rectangular display, which is kept horizontal) is affected by the phase function. So, a spiral-phase pattern displayed on the SLM, symmetrically illuminated by a Gaussian beam generates a symmetric OV beam when the input polarization is horizontal (H). The other polarization [i.e., vertical (V)] component of the incoming light does not see the phase function on the SLM and thus does not acquire the phase.

For an arbitrarily polarized incident beam of light, the output from the SLM results in a superposition of the phase-modulated H -polarized component and an unmodulated V -polarized component. The intensity ratio of the V - to H -polarized components, (I_V/I_H) , can be very easily controlled by just changing the angle of the input linear

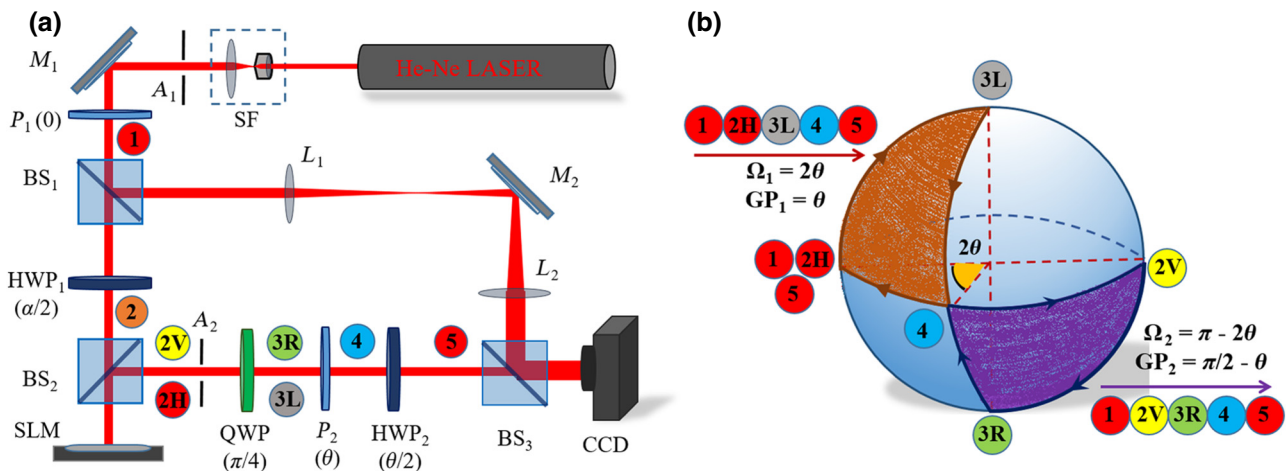


FIG. 1. (a) Schematic experimental setup for the generation of the off-axis optical vortex beam with a controlled relative intensity (RI) and GP variation between two orthogonal polarized component beams. The angle (α) of HWP_1 controls the RI of the $H-V$ polarization components and the angle (θ) of P_2 and HWP_2 ($\theta/2$) controls the GP. (b) Representing the evolution of the states of polarization at different places of the optical path on the Poincaré sphere. The enclosed solid angles (Ω) by the trajectories and the acquired PB GP of the two component beams are mentioned, which results in the PB GP difference of $|2\theta - \pi/2|$ between the component beams.

polarization by rotating a HWP without changing the total intensity.

A horizontally polarized beam of spatially filtered light from the laser is split into two equal intensity beams by the 50:50 beam splitter (BS_1). The polarization direction of the transmitted beam is then rotated by an angle (α) by a HWP₁ with fast axis placed at angle ($\alpha/2$) with respect to the horizontal polarization state. So, if the intensity of the transmitted beam after BS_1 is I_0 , then the intensity of the H -polarized component is $I_0 \cos^2(\alpha)$ and that of the V -polarized component is $I_0 \sin^2(\alpha)$. The intensity ratio of V - to H -polarized components is $I_V/I_H = \tan^2(\alpha)$. When this beam of light falls on the SLM displaying a phase function $\Phi(x, y)$, the amplitudes of the H - and V -polarized components become $\sqrt{I_0} \cos(\alpha) \exp[i\Phi(x, y)]$ and $\sqrt{I_0} \sin(\alpha)$, respectively, neglecting any overall propagation phase common to both the components. Although the intensity ratio still remains at $\tan^2(\alpha)$ there is now a phase difference of $\Phi(x, y)$ between the two polarization components.

Now a shift in PB GP between the two orthogonal linear polarization components is introduced using the sequential set of a QWP, a polarizer (P_2), and a HWP (HWP₂) combination. The state of polarization of each component is transformed to two orthogonal states of circular polarization before projecting to a linear polarized state. The QWP with fast axis at $\pi/4$ with respect to horizontal polarization, transforms the two linearly polarized beam into two circularly polarized beams of opposite handedness (state 3). The polarizer (P_2), whose pass axis makes an angle θ with the horizontal polarization, projects both the circular polarization states back to a linear polarization (state 4). Then a HWP, whose fast axis is at an angle $\theta/2$ to the horizontal polarization, takes the state of polarization back to horizontal linear polarization. The path traversed by each component on the Poincaré sphere is shown in Fig. 1(b). The two polarization components acquire different amounts of PB GP, with the difference corresponding to the relative phase shift δ . From Eqs. (1), (2), and Fig. 1(b) we get $\delta = |2\theta - \pi/2|$. So, the magnitude of the PB phase shift is, apart from a constant factor of $\pi/2$, equal to twice the angle made by the polarizer (θ) with respect to the horizontal polarization. This principle can also be employed to measure an unknown amount of acquired geometric phase difference just by measuring the rotation angle of the point singularity [14].

A sample-recorded interferogram and the steps involved in reconstructing the field profile of the object beam by Fourier fringe analysis [31] are schematically shown in Fig. 2. The expanded reference beam covers the entire active window of the CCD but the off-axis vortex beam covers less than one-third of the window and coincides with the central region of uniform intensity of the reference beam. It is ensured that they are at an angle with each other so that the fringes formed are diagonally oriented,

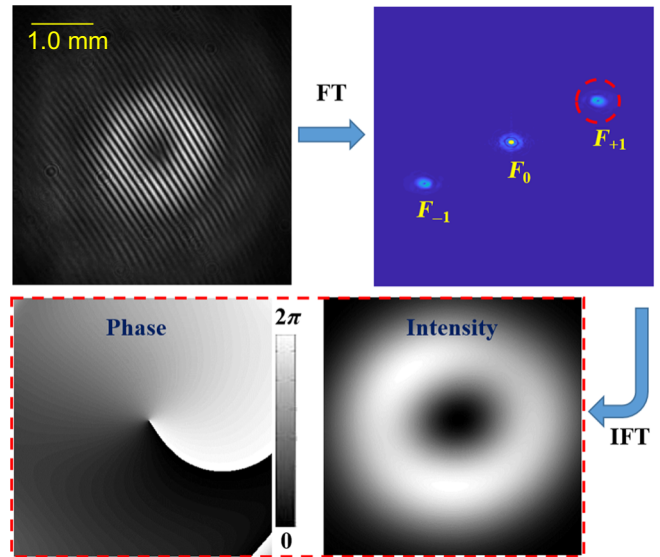


FIG. 2. Schematic of the Fourier fringe analysis of the experimentally recorded interferogram for reconstruction of the intensity and phase profile of the object beam. (I)FT, (inverse) Fourier transformation.

i.e., there is a carrier frequency both in x and y directions. First, the fast Fourier transformation of the interferogram is performed numerically, which gives three Fourier components: one zero-order dc component (F_0) and two first-order Fourier components ($F_{\pm 1}$). Selecting the positive first-order component (F_{+1}) and taking an inverse Fourier transform results in the full field profile from which the intensity and phase profile can be separately obtained.

IV. RESULTS AND DISCUSSION

The intensity distribution of the off-axis OV beams from experiment, as obtained from the reconstructed field profile after fringe analysis of the interferograms, are shown in Fig. 3. With change in the relative intensity of the component beams, due to the change in the angle of input linear polarization (α) on the SLM, the symmetric OV beam

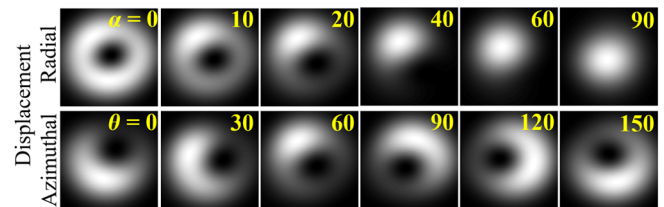


FIG. 3. Experimentally reconstructed intensity profiles from interferogram analysis for varying relative intensity of V and H polarization components by the input polarization angle α , giving radial displacement of vortex and for varying PB GP by the sequential QPH action on the component beams giving azimuthal displacement of vortex. α and θ are in degrees.

transforms to an off-axis OV beam and becomes a Gaussian beam when α becomes $\pi/2$. Whereas the azimuthal phase dependence of vortex beams results in a shift in the azimuthal coordinate of the off-axis vortex in the interference pattern by an amount equivalent to the introduced PB phase shift. The exact position of the point singularity can be obtained from the reconstructed phase profile from the recorded interferograms. To locate the position of point singularity to the accuracy of a pixel, numerically the pixel about which the phase changes by 2π is found by scanning over the beam cross section. The locus of the point singularity across the OV beam is shown in Fig. 4(a) for different values of the input plane polarization angle (α) with respect to the horizontal polarization and the pass-axis angle of the polarizer (θ) along which the circular polarization states are projected.

On studying the dependence of the vortex position on the relative intensities of the two component beams, the obtained radial displacement of the vortex with the angle of plane polarization of the input beam on the SLM is shown in Fig. 4(b). To verify the experimental nature, simulations are performed using the simple model given by Eq. (4) as well as using the realistic model of Eq. (7). The plot corresponding to the simulation using Eq. (4) qualitatively follows the experimental behavior. The model given by Eq. (7) gives a slightly closer match with the experimental plot.

For a fixed intensity ratio, the change of PB GP is observed to have the effect of changing only the azimuthal position of the singularity with a fixed radial position as shown in Fig. 4(c). This variation is linear with a slope of 2 as expected (because $\delta \propto 2\theta$) from the difference in PB GP acquired by the two polarization components. There emerges thus a correspondence between the polarizer's orientation (θ) and the azimuthal angle corresponding to the location of the off-axis vortex. This simple linear correspondence can be exploited to measure the geometric

phase acquired by a beam of light when passing through some number of polarizing components such as wave plates.

Next we focus on the amount of OAM carried by these off-axis vortex beams. An analytic expression for the average OAM per photon for a beam with an off-axis optical vortex of unit topological charge is provided by Kotlyar *et al.* [7],

$$l_{\text{th}} = \left[1 + \left(\frac{\sqrt{2}r_d}{\omega} \right)^2 \right]^{-1}. \quad (8)$$

Here, r_d represents the radial displacement of the vortex from the beam center and ω represents the beam radius.

Alperin *et al.* [32] have demonstrated a method to experimentally measure the OAM using a cylindrical lens and a CCD camera placed at the focal plane of the lens by capturing the intensity at the focal plane for two orthogonal orientation of the lens. Experiment and computer simulations are performed to model the measurement of OAM of the generated off-axis vortex beams, using the procedure mentioned in Ref. [32]. If the cylindrical lens (focal length f) transforms from (x, y) to (x', y) or to (x, y') depending on the orientation of the lens axis along horizontal (x) or vertical (y) direction, then the OAM along the z direction can be calculated using

$$l_{\text{exp}} = \frac{2\pi}{f\lambda} [\langle x'y \rangle - \langle xy' \rangle], \quad (9)$$

where the $x'y$ variance is given by

$$\langle x'y \rangle = \frac{\iint_{-\infty}^{\infty} |E(x', y)|^2 x'y dx' dy}{\iint_{-\infty}^{\infty} |E(x', y)|^2 dx' dy}$$

and similarly xy' variance can be defined.

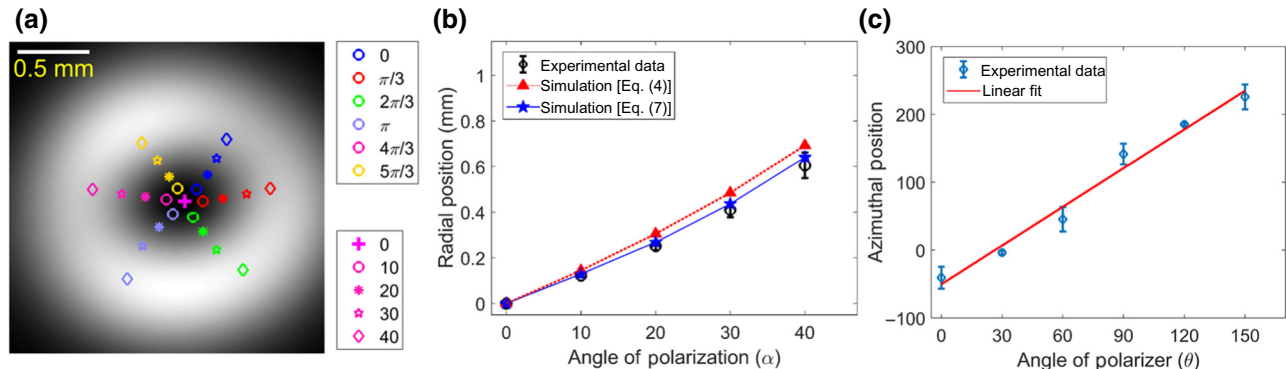


FIG. 4. (a) Trace of the position of phase singularity on varying relative intensity for different PB GP. Different colors correspond to different PB GP (in radian) and each different marker symbol represents a different relative intensity (values of α are in degrees). (b) Plot of radial displacement of vortex (r_d) versus angle of input polarization (α) from experiment and simulation using a realistic model and a simple model. (c) Plot of azimuthal vortex displacement for varying PB GP change due to change in the angle of pass axis for polarizer $P(\theta)$ and $HWP_2(\theta/2)$.

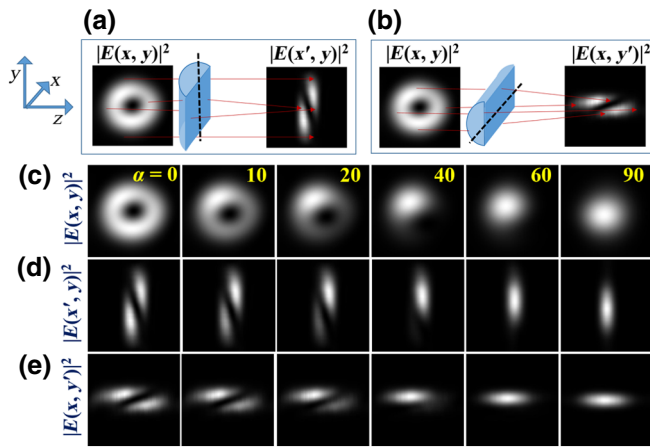


FIG. 5. Schematic for measurement of average OAM per photon of off-axis optical vortex beams from the intensity distributions at the focal plane of a cylindrical lens, for two orthogonal orientations of the lens axis: (a) axis vertical and (b) axis horizontal. (c) Intensity distributions before cylindrical lens $|E(x,y)|^2$; corresponding intensity distributions at focal plane of cylindrical lens: (d) $|E(x',y')|^2$ and (e) $|E(x,y')|^2$.

Intensity profiles before the cylindrical lens ($|E(x,y)|^2$) and at the focal plane of the cylindrical lens ($|E(x',y')|^2$ and $|E(x,y')|^2$) are shown in Fig. 5, for two orientations of the lens. The estimated OAM values by using Eq. (9) on the experimentally obtained intensity profiles, from the numerical simulation using Eq. (4) and that calculated using the analytic expression [Eq. (8)] depicts a close match as is shown in Fig. 6.

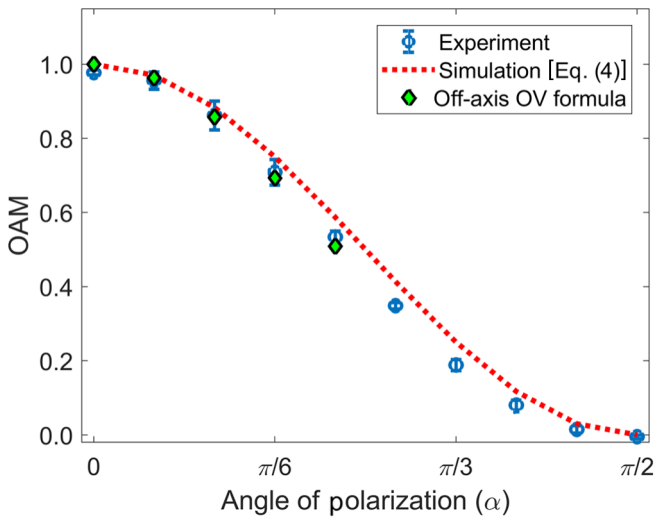


FIG. 6. Variation of the OAM with the varying intensity ratio of the component beams due to different input polarization angle (α): comparison of experimental, simulation and from analytic formula.

The distribution of TLM, which is proportional to the transverse component of the Poynting vector (S), is obtained from the reconstructed field profile, $\psi_r = f \exp(i\chi)$ of the beams, as per the formula [29], $S_{\perp} = f^2 \nabla \chi$. The distribution of TLM can thus be related to an intensity (f^2) weighted gradient of phase (χ). Calculating the gradient of phase along x and y directions, the x and y components of S_{\perp} are obtained, a vector plot of which reveals the transverse Poynting vector distribution. The magnitude of NTLM obtained from the integral of the TLM distribution across the beam, is calculated for various positions of the optical vortex. The variation of NTLM magnitude with change of the input polarization angle (α) on the SLM and also with resulting intensity ratio (I_g/I_{OV}) is shown in Figs. 7(a) and 7(b), respectively. The values obtained from simulated profiles and from the NTLM formula [Eq. (6a)] is plotted for comparison and shows close resemblance.

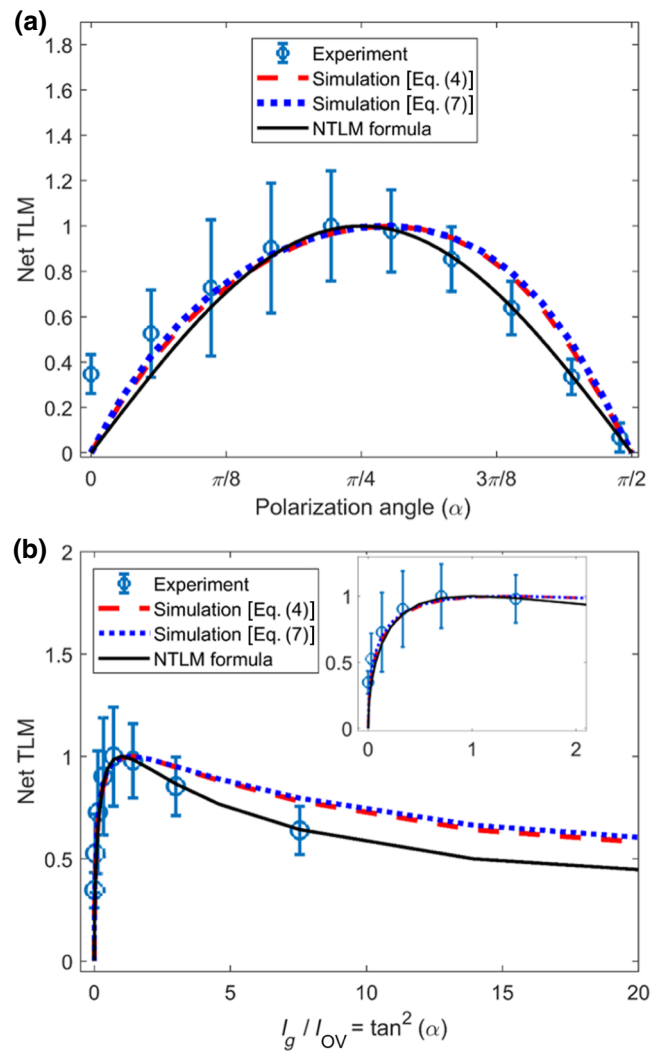


FIG. 7. (a) Variation of the NTLM with the angle of polarization (α) of the input beam on SLM. (b) Variation of the NTLM with the ratio of intensity of the Gaussian and OV beam.

The error bars for the experimental data plot of magnitude of NTLM with varying relative intensities of the component beams are obtained from the different sets of measurements due to different geometric phases that are introduced. The mean of the obtained NTLM value and deviation of the values from the mean are plotted as the data points and error bars, respectively. The reason for the error bar being large can be attributed to (i) the uncertainty in determining the locus of the point singularity from Fourier fringe analysis as the analysis space (in the Fourier domain) is also quantized by pixel and the possibility of larger error in finding the position of the singularity near low intensity region. (ii) The dependence of the precision in finding the radial displacement of the singularity with respect to the fringe orientation or the carrier-frequency component magnitude. (iii) Experimental asymmetry of the generated intensity profile.

While a symmetric OV beam has no NTLM, as is evident from the value of NTLM at $\alpha = 0$, beams with an off-axis vortex possess net TLM. The magnitude of NTLM increases to a peak and later falls off as we keep increasing the radial distance of the vortex from the beam axis. The peak corresponds to the situation where the displaced vortex lies along the maximum intensity circle of the original symmetric OV beam before superposition with a Gaussian beam, which corresponds to the case of two beams having equal intensity (i.e., at $\alpha = \pi/4$). The experimental plot matches well with the plot from the NTLM formula and from simulation. In Fig. 7(b), part of the plot is magnified in the inset for visual clarity.

The transverse Poynting vector distributions and the NTLM vector for different values of PB GP is shown in Fig. 8 for both experiment and simulation where the value of PB GP in degrees is mentioned at the top-right corner of each profile. The NTLM vector (shown by the red arrow) is always directed perpendicular to the vortex displacement [6], and the orientation of which depends on the sign of

the vortex topological charge. A PB GP shift between the superposed beams results in an azimuthal movement of the vortex, leading to rotation of the NTLM vector by an angle equivalent to the angular shift in the vortex position. It is noted that, for a fixed intensity ratio of the component beams the NTLM magnitude remains the same but its direction is rotated by rotating the off-axis vortex using controlled PB GP change.

The shift of the vortex can be explained from the interference of the plane-wave component of the two superposing beams as follows. The angular spectrum of a Gaussian beam of light reveals that it has a distribution of propagation vectors or k vectors in three dimensions, where each k vector implies a plane wave propagating in that particular vector direction. Thus it has only a longitudinal (k_z) and radial (k_r) component. A symmetric optical vortex beam, on the other hand, has a skewed distribution of k vectors and thus in addition to k_z and k_r has an azimuthal (k_ϕ) component [33]. The presence of k_ϕ is responsible for OAM arising along z (L_z). Individually both the beams have a perfect cylindrical symmetry, and the sum of all the k vectors for the individual beam give resultant only along the z direction. So they do not have any net TLM and the OAM of the symmetric vortex beam is intrinsic.

For the vortex beam, it can also be considered that the plane waves corresponding to the k vectors going along different azimuth have different phases, which for an OV of unit topological charge vary from 0 to 2π [33]. When superposed, the plane-wave components of the Gaussian beam and the vortex beam interfere. At the direction where the k vectors of the two beams have the same magnitude but corresponding plane waves have opposite phase, they will completely destructively interfere and the vortex position will shift to this new position across the beam. At some other point where they are in phase, interference is constructive and the intensity will be the highest. In other positions, it will be a partial constructive or destructive

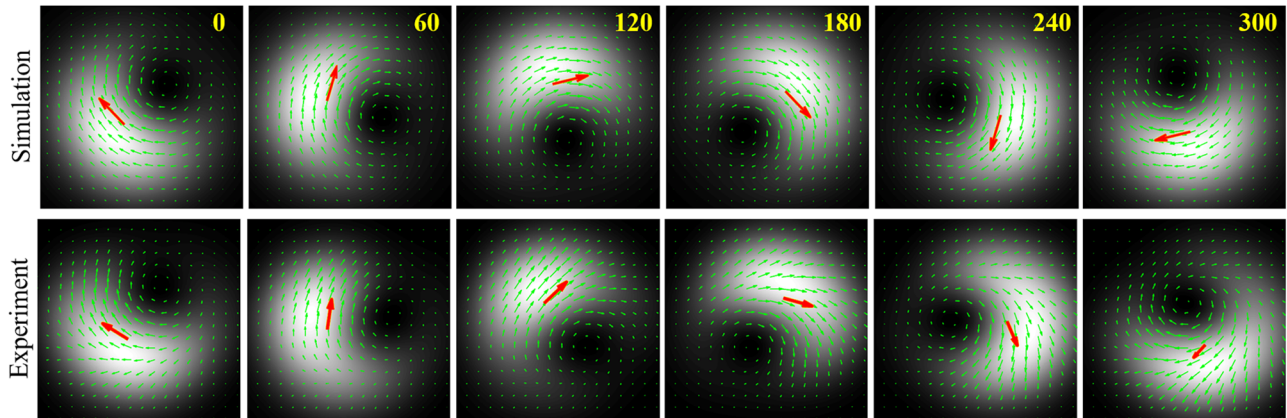


FIG. 8. Distributions of transverse Poynting vector (green arrows) along with the NTLM vector (red arrow) for off-axis vortex beams corresponding to different PB GP shifts (top-right corner, values in degrees) at a fixed intensity ratio.

interference. The superposition thus will have an asymmetric distribution and net k_r and k_ϕ (i.e., net TLM) components, which will result in an extrinsic OAM.

Changing the relative magnitude of k vectors, by varying the relative intensity of the component beams, moves the point vortex radially, whereas changing the relative phase of the component beams shifts move the point vortex azimuthally. In principle, the phase difference between the component beams can be introduced through a change in the dynamical phase as well, by varying the path length by a fraction of the wavelength in one of the branches in a two-path interferometer. However, this will be very sensitive to alignment and requires a very precise path delay. Use of the geometric phase, being far more robust compared to dynamic phase and wavelength independent, is naturally a favorable choice of implementing this phase difference. This tuning of magnitude and direction of extrinsic OAM due to the control of net TLM across the beam by off-axis vortex movement is the easiest and most robust way to achieve a fractional OAM with controllable extrinsic OAM. The same can be extended to any higher fractional OAM just by changing the spiral-phase order of the computer-generated holograms displayed on the SLM to higher integer topological charges.

The presented results can contribute in improving several applications of OAM beams where the control of vortex positions and vortex field asymmetry plays a crucial role. STED superresolution microscopy is one such application where the resolution is increased at the dark core of the vortex by suppressing fluorescence from the surrounding bright regions. To follow the region of interest in live-cell imaging [20], controlling the position of the vortex is of utmost importance. As demonstrated here, the method of tuning the vortex position in both radial and azimuthal directions across the beam with great flexibility and stability can improve the STED application significantly. Another potential application of the presented method can be in realizing OAM transfer to the BEC in atoms, which has recently been theorized for asymmetric OAM beam microscopic interaction [22]. It is theoretically predicted that due to the asymmetric nature of the OAM beam, multiple quantized circulations arise in the beam, which when transferred to the BEC, result in superposition of matter-vortex state and an increase in the Rabi frequency of quadrupole transition. Easily controlling the asymmetry as presented here can be helpful in the experimental realization of the theory.

V. CONCLUSIONS

The superposition of a Gaussian beam onto an OV beam with a vortex at the center of the beam results in an asymmetric OV beam with an off-axis vortex. In this Paper, it is shown that the average orbital angular momentum and net transverse linear momentum of the

beam depend on the displacement of the vortex from the center. While the radial displacement of the vortex is controlled by altering the relative intensities of the superposed beams, the azimuthal co-ordinate is manipulated by introducing a relative phase in terms of Pancharatnam-Berry geometric phase. The polarization states of both the polarization components in the superposed beams are altered along two different closed paths on the Poincaré sphere to introduce a suitable Pancharatnam-Berry geometric phase in a controlled manner. The magnitude of the net transverse linear momentum, giving rise to extrinsic OAM, is controlled by moving the off-axis vortex radially and the direction of net TLM is rotated by a controlled geometric phase change. Exercising precise and robust control of the perfect dark region of the point vortex can enable flexibility in choosing the region of interest in superresolution microscopy while controlling the OAM can be useful in manipulating trapped microparticles. This easy method of measuring geometric phase in the proposed single-path configuration can be employed to other sensitive applications.

ACKNOWLEDGMENTS

We are grateful to the anonymous referees for their helpful comments and suggestions in improving the quality of this Paper. We thank Mr Arabinda Mandal for his help in the experimental data acquisition. S. Maji gratefully acknowledges IIT Kharagpur and MHRD, Govt. of India for the fellowship. This research work is supported by Department of Science and Technology (DST), Ministry of Science and Technology India (INSPIRE Faculty Award/2013/PH-62) and Indian Institute of Technology Kharagpur (IIT/SRIC/PHY/VBC/2014-15/43).

S.M. and P.J. contributed equally in this work.

-
- [1] L. Allen, M. W. Beijersbergen, R. J. C. Spreeuw, and J. P. Woerdman, Orbital angular momentum of light and the transformation of Laguerre-Gaussian laser modes, *Phys. Rev. A* **45**, 8185 (1992).
 - [2] K. T. Gahagan and G. A. Swartzlander, Optical vortex trapping of particles, *Opt. Lett.* **21**, 827 (1996).
 - [3] A. E. Willner, H. Huang, Y. Yan, Y. Ren, N. Ahmed, G. Xie, C. Bao, L. Li, Y. Cao, Z. Zhao, J. Wang, M. P. J. Lavery, M. Tur, S. Ramachandran, A. F. Molisch, N. Ashrafi, and S. Ashrafi, Optical communications using orbital angular momentum beams, *Adv. Opt. Photon.* **7**, 66 (2015).
 - [4] S. W. Hell and J. Wichmann, Breaking the diffraction resolution limit by stimulated emission: Stimulated-emission-depletion fluorescence microscopy, *Opt. Lett.* **19**, 780 (1994).
 - [5] S. Furhapter, A. Jesacher, S. Bernet, and M. Ritsch-Marte, Spiral phase contrast imaging in microscopy, *Opt. Express* **13**, 689 (2005).

- [6] S. Maji, A. Mandal, and M. Brundavanam, Gouy phase-assisted topological transformation of vortex beams from fractional fork holograms, *Opt. Lett.* **44**, 2286 (2019).
- [7] V. V. Kotlyar, A. A. Kovalev, and A. P. Porfirev, Asymmetric gaussian optical vortex, *Opt. Lett.* **42**, 139 (2017).
- [8] R. Zambrini and S. M. Barnett, Quasi-Intrinsic Angular Momentum and the Measurement of its Spectrum, *Phys. Rev. Lett.* **96**, 113901 (2006).
- [9] A. T. O’Neil, I. MacVicar, L. Allen, and M. J. Padgett, Intrinsic and Extrinsic Nature of the Orbital Angular Momentum of a Light Beam, *Phys. Rev. Lett.* **88**, 053601 (2002).
- [10] S. S. R. Oemrawsingh, E. R. Eliel, G. Nienhuis, and J. P. Woerdman, Intrinsic orbital angular momentum of paraxial beams with off-axis imprinted vortices, *J. Opt. Soc. Am. A* **21**, 2089 (2004).
- [11] M. V. Berry, Paraxial beams of spinning light, In *Singular optics*, edited by M. S. Soskin, Proc. No. 3487 (SPIE, Frunzenskoe, Crimea, 1998).
- [12] S. N. Alperin and M. E. Siemens, Angular Momentum of Topologically Structured Darkness, *Phys. Rev. Lett.* **119**, 203902 (2017).
- [13] A. Vaziri, G. Weihs, and A. Zeilinger, Superpositions of the orbital angular momentum for applications in quantum experiments, *J. Opt. B: Quantum Semiclass. Opt.* **4**, S47 (2002).
- [14] E. J. Galvez, P. R. Crawford, H. I. Sztul, M. J. Pysher, P. J. Haglin, and R. E. Williams, Geometric Phase Associated with Mode Transformations of Optical Beams Bearing Orbital Angular Momentum, *Phys. Rev. Lett.* **90**, 203901 (2003).
- [15] S. Pancharatnam, Generalized theory of interference, and its applications, *Proc. Indian Acad. Sci. (A)* **44**, 247 (1956).
- [16] M. Berry, The adiabatic phase and Pancharatnam’s phase for polarized light, *J. Mod. Opt.* **34**, 1401 (1987).
- [17] P. Jacob, S. Maji, and M. M. Brundavanam, Experimental measurement of pancharatnam-berry phase by interferometry using an optical vortex beam (2019), int. Conf. on OAM (unpublished).
- [18] S.-L. Zhu and P. Zanardi, Geometric quantum gates that are robust against stochastic control errors, *Phys. Rev. A* **72**, 020301(R) (2005).
- [19] K. Y. Bliokh, F. Rodriguez-Fortuno, F. Nori, and A. Zayats, Spin-orbit interactions of light, *Nat. Photonics* **9**, 796 (2015).
- [20] B. Hein, K. I. Willig, and S. W. Hell, Stimulated emission depletion (STED) nanoscopy of a fluorescent protein-labeled organelle inside a living cell, *Proc. Natl. Acad. Sci.* **105**, 14271 (2008).
- [21] P. K. Mondal, B. Deb, and S. Majumder, Angular momentum transfer in interaction of Laguerre-Gaussian beams with atoms and molecules, *Phys. Rev. A* **89**, 063418 (2014).
- [22] S. Das, A. Bhowmik, K. Mukherjee, and S. Majumder, Transfer of orbital angular momentum superposition from asymmetric Laguerre-Gaussian beam to Bose-Einstein condensate, *J. Phys. B: At. Mol. Opt. Phys.* (in press) (2019).
- [23] M. V. Berry, Quantal phase factors accompanying adiabatic changes, *Proc. R. Soc. A* **392**, 45 (1984).
- [24] D. M. Tong, E. Sjoqvist, L. C. Kwek, and C. H. Oh, Kinematic Approach to the Mixed State Geometric Phase in Nonunitary Evolution, *Phys. Rev. Lett.* **93**, 080405 (2004).
- [25] R. Bhandari and J. Samuel, Observation of Topological Phase by Use of a Laser Interferometer, *Phys. Rev. Lett.* **60**, 1211 (1988).
- [26] R. Bhandari, Polarization of light and topological phases, *Phys. Rep.* **281**, 1 (1997).
- [27] F. Flossmann, U. T. Schwarz, M. Maier, and M. R. Dennis, Polarization Singularities from Unfolding an Optical Vortex Through a Birefringent Crystal, *Phys. Rev. Lett.* **95**, 253901 (2005).
- [28] M. J. Padgett, F. M. Miatto, M. P. J. Lavery, A. Zeilinger, and R. W. Boyd, Divergence of an orbital-angular-momentum-carrying beam upon propagation, *New J. Phys.* **17**, 023011 (2015).
- [29] S. Maji and M. Brundavanam, Topological transformation of fractional optical vortex beams using computer generated holograms, *J. Opt.* **20**, 045607 (2018).
- [30] V. V. Kotlyar, A. A. Kovalev, S. N. Khonina, R. V. Skidanov, V. A. Soifer, H. Elfstrom, N. Tossavainen, and J. Turunen, Diffraction of conic and gaussian beams by a spiral phase plate, *Appl. Opt.* **45**, 2656 (2006).
- [31] M. Takeda, H. Ina, and S. Kobayashi, Fourier transform method of fringe-pattern analysis for computer based topography and interferometry, *J. Opt. Soc. Am.* **72**, 156 (1982).
- [32] S. N. Alperin, R. D. Niederriter, J. T. Gopinath, and M. E. Siemens, Quantitative measurement of the orbital angular momentum of light with a single, stationary lens, *Opt. Lett.* **41**, 5019 (2016).
- [33] K. Y. Bliokh, I. Ivanov, G. Guzzinati, L. Clark, R. V. Boxem, A. Beche, R. Juchtmans, M. Alonso, P. Schattschneider, F. Nori, and J. Verbeeck, Theory and applications of free-electron vortex states, *Phys. Rep.* **690**, 1 (2017).